Article
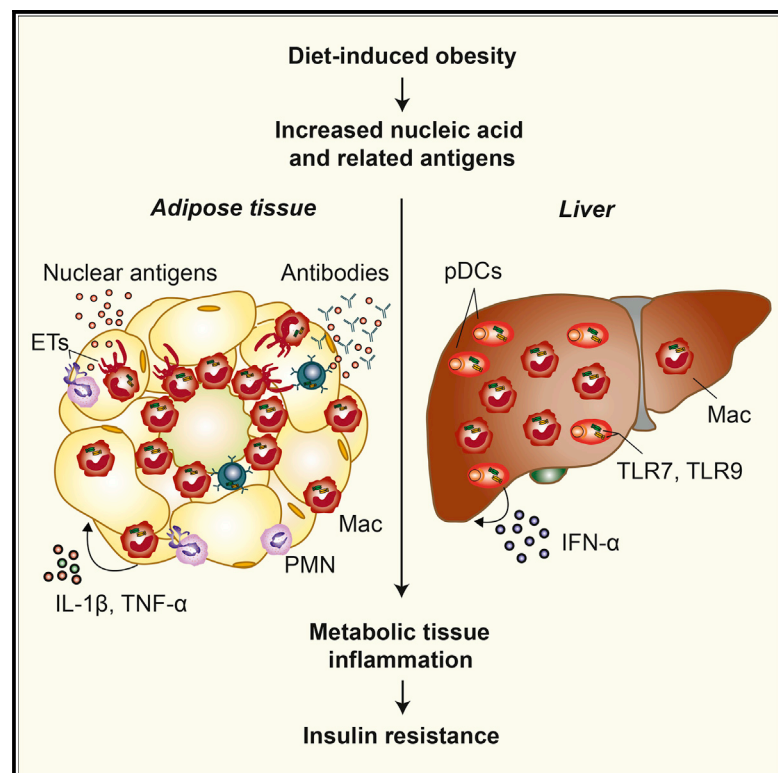
# Nucleic Acid-Targeting Pathways Promote Inflammation in Obesity-Related Insulin Resistance

## Graphical Abstract

## Authors

Xavier S. Revelo, Magar Ghazarian, Melissa Hui Yen Chng, ..., Edgar Engleman, Shawn Winer, Daniel A. Winer

## Correspondence

xrevelo@uhnresearch.ca (X.S.R.),
dan.winer@uhn.ca (D.A.W.)

## In Brief

Revelo et al. show that diet-induced obesity promotes excess release and diminished clearance of nucleic acid and related antigens, with appearance of autoantibodies. Aberrant handling of nucleic acids activates VAT macrophages and liver pDCs via TLR7/9 to promote inflammation. Nucleic acid-sensing pathways may represent therapeutic targets for obesity-related metabolic disease.

## Highlights

- Obesity promotes increased release and decreased clearance of nucleic acid antigens

- Aberrant handling of nucleic acid and related antigens results in autoantibodies

- Excess nucleic acids worsen metabolism through VAT macrophages and liver pDCs

- Inhibiting TLR7/9 improves obesity-related inflammation and glucose homeostasis

CrossMark

CellPress

OPEN
ACCESS
CellPress

Cell Reports
# Article

# Nucleic Acid-Targeting Pathways Promote Inflammation in Obesity-Related Insulin Resistance

Xavier S. Revelo,[1,*] Magar Ghazarian,[1] Melissa Hui Yen Chng,[2] Helen Luck,[1] Justin H. Kim,[1] Kejing Zeng,[1,3] Sally Y. Shi,[1] Sue Tsai,[1] Helena Lei,[1] Justin Kenkel,[2] Chih Long Liu,[4] Stephanie Tangsombatvisit,[4] Hubert Tsui,[5] Corneliu Sima,[6] Changting Xiao,[7] Lei Shen,[8] Xiaoying Li,[9] Tianru Jin,[1] Gary F. Lewis,[7] Minna Woo,[1,7] Paul J. Utz,[4] Michael Glogauer,[10] Edgar Engleman,[2] Shawn Winer,[1,11,12,14] and Daniel A. Winer[1,5,12,13,14,*]

[1]Division of Cellular and Molecular Biology, Diabetes Research Group, Toronto General Research Institute (TGRI), University Health Network, Toronto, ON M5G 1L7, Canada
[2]Department of Pathology, Stanford University School of Medicine, Palo Alto, CA 94305, USA
[3]Department of Endocrinology and Metabolism, Third Affiliated Hospital of Sun Yat-Sen University, Guangzhou 510630, China
[4]Department of Medicine, Division of Immunology and Rheumatology, Stanford University School of Medicine, Palo Alto, CA 94305, USA
[5]Department of Pathology, University Health Network, Toronto, ON M5G 2C4, Canada
[6]Department of Applied Oral Sciences, The Forsyth Institute, Cambridge, MA 02142, USA
[7]Division of Endocrinology and Metabolism, Department of Medicine, University Health Network, Toronto, ON M5G 2C4, Canada
[8]Shanghai Institute of Immunology, Shanghai Jiao Tong University School of Medicine, Shanghai 200240, China
[9]Department of Endocrinology, Zhongshan Hospital, Fudan University, Shanghai 200011, China
[10]Faculty of Dentistry, University of Toronto, Matrix Dynamics Group, Toronto, ON M5G 1G6, Canada
[11]Department of Laboratory Medicine, St. Michael's Hospital, Toronto, ON M5B 1W8, Canada
[12]Department of Laboratory Medicine and Pathobiology, University of Toronto, Toronto, ON M5S 1A8, Canada
[13]Department of Immunology, University of Toronto, Toronto, ON M5S 1A8, Canada
[14]Co-senior author
*Correspondence: xrevelo@uhnresearch.ca (X.S.R.), dan.winer@uhn.ca (D.A.W.)
http://dx.doi.org/10.1016/j.celrep.2016.06.024

## SUMMARY

Obesity-related inflammation of metabolic tissues, including visceral adipose tissue (VAT) and liver, are key factors in the development of insulin resistance (IR), though many of the contributing mechanisms remain unclear. We show that nucleic-acid-targeting pathways downstream of extracellular trap (ET) formation, unmethylated CpG DNA, or ribonucleic acids drive inflammation in IR. High-fat diet (HFD)-fed mice show increased release of ETs in VAT, decreased systemic clearance of ETs, and increased autoantibodies against conserved nuclear antigens. In HFD-fed mice, this excess of nucleic acids and related protein antigens worsens metabolic parameters through a number of mechanisms, including activation of VAT macrophages and expansion of plasmacytoid dendritic cells (pDCs) in the liver. Consistently, HFD-fed mice lacking critical responders of nucleic acid pathways, Toll-like receptors (TLR)7 and TLR9, show reduced metabolic inflammation and improved glucose homeostasis. Treatment of HFD-fed mice with inhibitors of ET formation or a TLR7/9 antagonist improves metabolic disease. These findings reveal a pathogenic role for nucleic acid targeting as a driver of metabolic inflammation in IR.

## INTRODUCTION

Insulin resistance (IR) precedes type 2 diabetes and is a key feature of obesity-related metabolic syndrome. Multiple factors contribute to insulin sensitivity, but inflammation of visceral adipose tissue (VAT) and liver, leading to chronic release of pro-inflammatory cytokines, is a major contributor (Osborn and Olefsky, 2012). Within VAT, macrophages, T cells, B cells, innate lymphoid cells, eosinophils, and neutrophils take part in this process (Mathis, 2013). Neutrophils promote IR in high-fat diet (HFD)-fed mice through secretion of elastase (Talukdar et al., 2012) and myeloperoxidase (Wang et al., 2014a). In addition to their traditional antimicrobial mechanisms, neutrophils can release extracellular traps (ETs), composed of nucleic acids and antimicrobials, to entrap pathogens and limit infection (Brinkmann et al., 2004). Macrophages also extrude ET-like structures (Chow et al., 2010; Liu et al., 2014; Webster et al., 2010). Recently, these macrophage ET-like structures have been identified within crown-like structures (CLSs) in mammary gland subcutaneous adipose tissue (SAT) of mice (Mohanan et al., 2013), though this process needs further characterization.

Aberrant production and reduced clearance of ETs can lead to accumulation of immunogenic self-antigens and promotion of autoimmune diseases, such as systemic lupus erythematosus (SLE) (Garcia-Romo et al., 2011; Hakkim et al., 2010) and type 1 diabetes (Diana et al., 2013; Wang et al., 2014b). Remarkably, SLE is highly linked to metabolic syndrome (Demir et al., 2016; Parker et al., 2015), with enhanced development of IR (Parker and Bruce, 2010). In SLE, aberrant antibody targeting of nucleic acids potentiates inflammation through Toll-like receptor (TLR)7
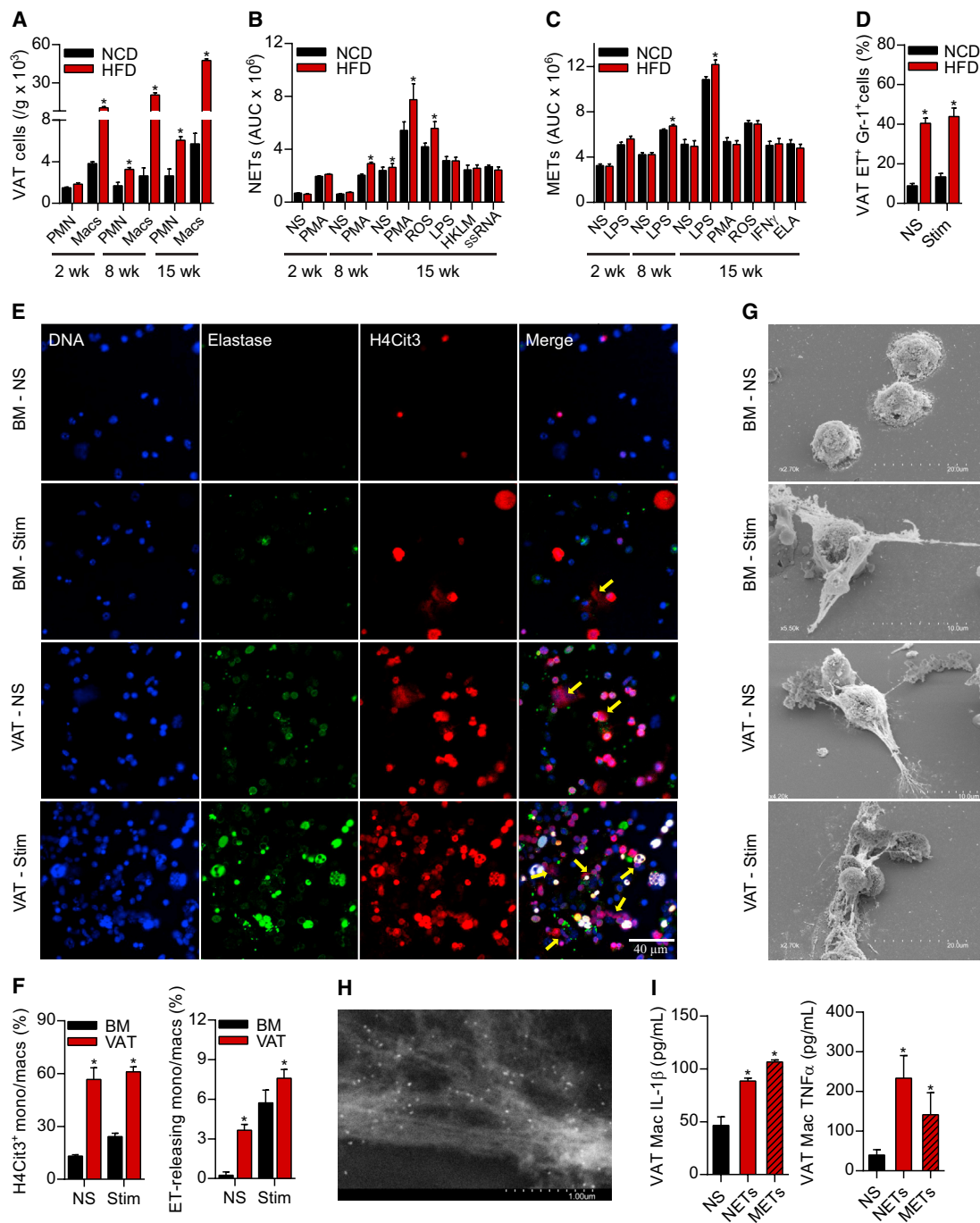
**Figure 1. Aberrant Production of ETs during HFD Feeding**

(A) Absolute number of CD11b+Ly6g+ neutrophils and F480+ macrophages in the visceral adipose tissue (VAT) of mice fed either a normal control diet (NCD) or a high-fat diet (HFD) for 2, 8, and 15 weeks is shown (n = 10 mice, three experiments, *p < 0.05).

(B) Release of extracellular traps (ETs) by BM neutrophils harvested from mice fed an NCD or HFD for 2, 8, and 15 weeks, left non-stimulated (NS) or activated with phorbol 12-myristate, 13-acetate (PMA) for 6 hr. At the 15-week time point, cells also were stimulated with reactive oxygen species (ROS), *E. coli* lipopolysaccharide (LPS), heat-killed *Listeria monocytogenes* (HKLM), and single-stranded RNA oligonucleotides (ssRNA).

(C) Release of ETs by BM monocytes harvested from mice fed an NCD or HFD for 2, 8, and 15 weeks, left NS or activated with LPS for 6 hr. At the 15-week time point, cells also were stimulated with PMA, ROS, interferon-γ (IFNγ), or elastase (ELA).

(B and C) ETs were quantified with Sytox Green staining and fluorescence measurements were taken every 30 min. Data represent the area under the curve (AUC) calculated from plotted fluorescent measurements over time (n = 6 mice per group, *p < 0.05).

*(legend continued on next page)*

and/or TLR9 activation in macrophages (in mice), B cells, and plasmacytoid dendritic cells (pDCs) (Liu and Davidson, 2012). Neutrophil ETs (NETs) also have been shown to increase the production of proinflammatory cytokines by CD4$^+$ and CD8$^+$ T cells (Tillack et al., 2012) and act on monocytes in lupus to activate the NLRP3 inflammasome (Kahlenberg et al., 2013). Notably, a recent study has shown that types 1 and 2 diabetes predispose neutrophils to release increased NETs, which delays wound healing in humans and mice (Wong et al., 2015). However, a pathophysiological role for ETs in promoting glucose intolerance during obesity is unknown.

In addition to endogenous sources of nucleic acids, TLR9 ligands from exogenous sources, including unmethylated CpG, may contribute to inflammation in obesity. Indeed, obesity is associated with altered composition of the gut microbiota, and this dysbiosis can influence IR (Cani et al., 2008). In fact, some of the systemic inflammation associated with IR is thought to result from increased serum levels of leaked gut bacterial products, such as lipopolysaccharide (LPS), and unmethylated CpG DNA, which may exert effects systemically or locally in VAT or liver (Henao-Mejia et al., 2012).

Here we show that alterations in nucleic acid-targeting pathways occur in HFD-induced obesity and impact the development of metabolic disease. Downstream immunological responses to nucleic acids are important drivers of inflammation in obesity-related IR, and they represent a source of antigenic targets and potential therapies in IR.

## RESULTS

### HFD Promotes Increased ET Formation

Because ET formation has been implicated in the pathogenesis of several inflammatory diseases, we hypothesized ET release would be augmented in response to HFD feeding. First, we determined the presence of ET-releasing immune cells, such as neutrophils and macrophages within VAT, during the course of HFD feeding. Compared with normal control diet (NCD)-fed mice, the number of VAT neutrophils substantially increased after 8 and 15 weeks, while VAT macrophage numbers increased following 2, 8, and 15 weeks of HFD feeding (Figure 1A).

To assess the effects of HFD on ET production from a systemic hematolymphoid source, we analyzed ET formation by bone marrow (BM) neutrophils and monocytes using the extracellular DNA dye Sytox and by immunostaining of citrullinated histones. Histone citrullination is required for chromatin decondensation during ETosis, and certain patterns of histone citrullination are considered specific markers of ET formation (Wang et al.,

2009). Compared with NCD-fed controls, BM neutrophils from mice fed a HFD for 8 and 15 weeks released increased amounts of NETs when stimulated with phorbol 12-myristate 13-acetate (PMA) and reactive oxygen species (ROS), but not upon stimulation with several TLR agonists (Figure 1B). HFD feeding also increased the release of BM monocyte/macrophage ET-like structures (METs) at 8 and 15 weeks of dietary treatment, but only in LPS-stimulated cells (Figure 1C), suggesting fundamental differences between the stimulation process leading to NET and MET formation. We confirmed that our fluorescence-based assay was specific for extracellular DNA, since the addition of DNase-1 abolished the fluorescence signal (Figure S1A) and mass spectrometry (MS) analysis showed that the proteins associated with these NETs and METs included histones and several antimicrobials (Data S1), as previously reported (Urban et al., 2009).

We next assessed whether diet-induced obesity (DIO) results in increased release of ETs in active metabolic tissues, such as inflamed VAT. Stromal vascular cells (SVCs) harvested from VAT of NCD- and HFD-fed mice were stained for histone 3, a component of ETs. Immunostaining for histone 3 showed intracytoplasmic and extracellular translocation of histone protein characteristic of ETosis (Figure S1B). The percentage of Gr-1$^+$ SVCs, which include primarily neutrophils and some macrophages, releasing ETs was dramatically increased in HFD-fed mice compared with NCD-fed controls in non-stimulated and stimulated states (Figure 1D). To confirm that increased histone 3 in VAT of HFD-fed mice is indicative of ET formation, adipose tissue sections from NCD- and HFD-fed mice were stained for histone 4-citrulline 3 (H4-Cit3). Compared with NCD controls, VAT from HFD-fed mice showed increased H4-Cit3 in the nucleus and cytoplasm of neutrophils and macrophages and in CLS near adipocytes (Figure S2A). VAT of obese patients with a previous diagnosis of type 2 diabetes also showed positive staining of H4-Cit3, suggesting that ETs may be present during obesity-induced VAT inflammation in humans, although this finding needs future characterization (Figure S2A).

Because proinflammatory macrophages play a pivotal role in chronic low-grade inflammation during obesity and are far more numerous in VAT compared with neutrophils, we next investigated whether HFD alters the production of ETs by monocyte/macrophages in VAT. Monocyte/macrophages from BM and VAT of HFD-fed mice were stimulated with LPS and immunostained for H4-Cit3 and elastase (Figure 1E; Figure S2B). Compared with BM cells, VAT macrophages had increased percentages of both H4-Cit3$^+$ and ET-releasing cells

(D) Percentage of ET-releasing, granulocyte receptor (Gr)-1$^+$ stromal vascular cells (SVCs) harvested from VAT of either NCD- or HFD- fed mice is shown (triplicates, n = 10 mice per group, *p < 0.05).

(E) Representative immunofluorescence images showing DNA (blue), ELA (green), and H4Cit3 (red) in BM monocytes and VAT macrophages, left NS or after a 4-hr incubation with LPS (scale bar, 40 μm). Yellow arrows indicate ETs.

(F) Quantification of H4Cit3$^+$ cells (left) and ET-releasing monocytes/macrophages (right) in immunofluorescence images is shown (n = 10 mice, two experiments, *p < 0.05).

(G) Scanning electron microscopy (SEM) images show BM and VAT macrophages left NS or after incubation with LPS for 4 hr.

(H) SEM image shows immunogold-labeled H4Cit3 in ETs released by an LPS-stimulated macrophage from the VAT of HFD-fed mice.

(I) Production of IL-1β (left) and TNF-α (right) by LPS-primed VAT macrophages from HFD-fed mice following exposure to purified NETs and METs (n = 10 mice, three experiments, *p < 0.05). Error bars show mean ± SEM.

See also Figures S1, S2, and S3 and Data S1.
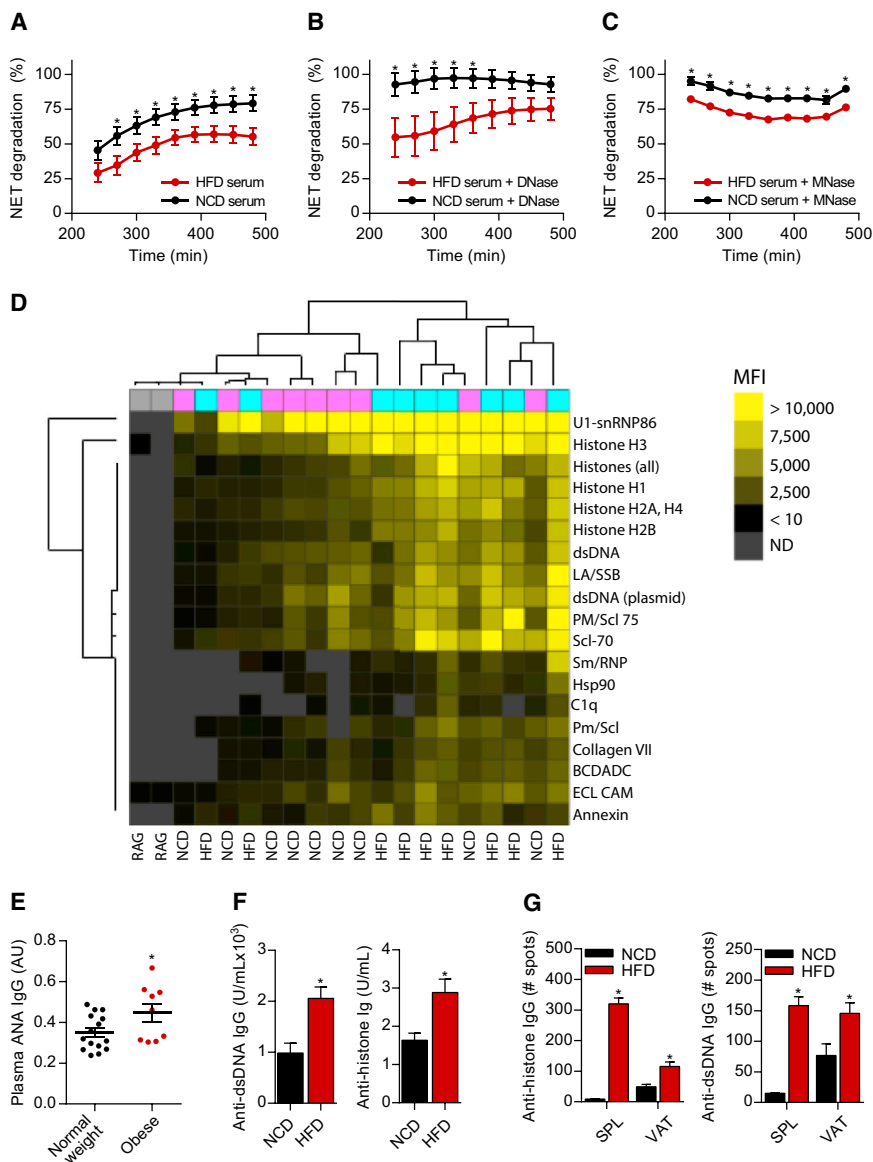
**Figure 2. HFD-Induced Obesity Promotes Defective ET Degradation and Elevated Autoantibody Titers against Nucleic Acids and Related Antigens**

(A–C) ET degradation by serum alone (A), supplemented with DNase (B), or MNase (C) collected from mice fed either an NCD or HFD for 15 weeks is shown (n = 6, *p < 0.05).

(D) Heatmap of mean fluorescence intensity (MFI) showing IgM antibody levels against self-antigens in serum from NCD- and HFD-fed mice (n = 9). Antibody levels are in shades of yellow with highest titers as bright yellow (bright yellow represents an MFI $\geq$ 10,000). The heatmap displays antibody reactivity significantly associated with HFD versus NCD feeding, as assessed by the SAM algorithm (q < 0.001) and grouped by Euclidean distance hierarchical clustering. RAG-deficient mice were used as negative controls (far left lanes).

(E) Relative plasma levels of anti-nuclear antibodies (ANAs) in normal weight (n = 15) and overweight/obese (n = 9) patients (*p < 0.05). Data represent absorbance a.u.

(F) Plasma concentrations of anti-dsDNA (left) and anti-histone (right) IgG determined by ELISA in mice fed an NCD or HFD for 15 weeks are shown (n = 7, *p < 0.05).

(G) ELISPOT analysis of VAT SVCs enriched for B cells from mice fed an NCD or HFD for 15 weeks seeded onto plates coated with histone (left) and dsDNA (right, n = 14 mice each, two experiments, *p < 0.05). Error bars show mean ± SEM.

See also Figure S4 and Table S1.

the amounts of the IL-1β and TNF-α in the supernatants of VAT macrophages (Figure 1I), suggesting a direct link between excessive ET release and VAT macrophage activation during DIO. Collectively, these results indicate that HFD-derived VAT macrophages have increased ability to release ETs, compared with their BM precursors, and that ETs have potential to fuel local immune activation and cytokine production in metabolic tissue, revealing a mechanism of inflammation in VAT during obesity.

(Figure 1F). Notably, VAT macrophages showed increased H4-Cit3 staining and MET release, even in the absence of stimuli (Figure 1F), suggesting an activated phenotype in vivo. Furthermore, scanning electron microscopy (SEM) images of BM monocytes and VAT macrophages showed the typical extracellular fibers (Figure 1G; Figure S3), corroborating their ability to form ET-like structures. In addition, immunogold labeling of ET-releasing VAT macrophages for SEM showed H4-Cit3 concentrated in these structures (Figure 1H), confirming the formation of METs.

We next investigated whether NETs and METs can directly activate VAT macrophages, promoting the release of inflammatory cytokines IL-1β and TNF-α. VAT macrophages from HFD-fed mice were exposed for 2 hr to ET-associated components produced by BM neutrophils and macrophages (Urban et al., 2009). Both NET- and MET-associated components increased

## Defective ET Degradation and Autoantibody Production against Nucleic Acid-Related Antigens Are Hallmarks of DIO

Since ETs are increased systemically and locally in metabolic tissues during HFD feeding, and ineffective systemic clearance of ETs promotes the production of antibodies against self-antigens (Hakkim et al., 2010), we next sought to investigate whether systemic ET clearance and autoantibody production are altered in HFD-fed mice. After ETs were induced ex vivo, they were incubated with serum from mice fed either an NCD or HFD, and ET degradation was determined. Compared with serum from NCD controls, serum from HFD mice showed reduced capacity to degrade ETs (Figure 2A). To determine whether this ineffective

ET degradation was due to low serum DNase activity, exogenous DNase was added to the reactions. DNase spiking increased ET clearance in NCD serum to levels close to 100%; however, it only marginally improved clearance by HFD serum (Figure 2B). Indeed, treatment of HFD-fed mice with DNase had no effect on glucose tolerance (Figure S4). Therefore, reduced ET degradation in HFD mice is not caused by low DNase activity, but it is likely due to the presence of either DNase inhibitors or the physical protection of ETs against DNase. To further clarify these possibilities, we spiked serum from NCD and HFD mice with the non-specific nuclease micrococcal nuclease (MNase). Spiking HFD serum with MNase did not restore ET degradation relative to NCD serum (Figure 2C), suggesting protection of ETs from nuclease activity.

We next proposed that the aberrant production and defective clearance of ETs would elicit increased production of autoantibodies against components of ETs. Using a custom-made array (Price et al., 2013), we screened serum from HFD-fed mice for >200 autoantibodies, and we detected a group of auto-antigens that differed between NCD and HFD mice, including the U1 small nuclear ribonucleoprotein (RNP) 86; the histones H1, H2A, H2B, and H3; and double-stranded DNA (dsDNA) (Figure 2D). Remarkably, overlapping findings also are seen in a cohort of normal weight versus overweight/obese human subjects (clinical parameters summarized in Table S1). Specifically, the levels of anti-nuclear antibodies (ANAs), which include autoantibodies against dsDNA, histones, and RNPs, are increased in the plasma of overweight or obese humans compared with normal weight subjects (Figure 2E). In agreement with the array findings, we validated the plasma levels of anti-dsDNA and anti-histone IgGs with ELISA, and these autoantibodies were increased in HFD-fed mice (Figure 2F). To assess whether this adaptive immune response against nucleic acid-related antigen occurs both systemically and locally in VAT, total splenocytes and B cell-enriched VAT-derived SVCs from NCD and HFD mice were assessed by ELISPOT for B cell production of IgG against histone and dsDNA. IgG production against dsDNA and histone 2A by splenic and VAT B cells was strikingly augmented in HFD-fed mice compared with NCD-fed controls (Figure 2G). These data suggest that increased autoantibody production against nucleic acid-related antigens occurs systemically in hematolymphoid organs and locally in VAT, consistent with a role for targeting of nucleic acid-related antigen during HFD feeding.

### Nucleic Acid-Sensing Receptors Regulate Glucose Homeostasis and Insulin Signaling

We next investigated the roles of the downstream target receptors TLR7 and TLR9 in DIO-related IR. These TLRs often gain access to nucleic acids after cell-mediated uptake of antibody-antigen complexes, where they recognize nucleoprotein antigens such as RNPs (TLR7) (Savarese et al., 2006) and dsDNA (TLR9) (Martin and Elkon, 2005). First, we asked whether ET-associated components can be sensed by TLR7 and TLR9 in VAT macrophages. Macrophages purified from the VAT of HFD-fed wild-type (WT), TLR7$^{-/-}$, and TLR9$^{-/-}$ mice were exposed for 2 hr to ET-associated components to determine their release of proinflammatory cytokines. Compared with VAT macrophages from WT mice, those from TLR7$^{-/-}$ and TLR9$^{-/-}$ mice showed

reduced release of IL-1β and TNF-α (Figure 3A), suggesting that these nuclear receptors are partly responsible for the activity of macrophages observed after treatment with ET components.

Therefore, we next determined the effects of genetic deletion of TLR7 and TLR9 on metabolic parameters in NCD- and HFD-fed mice. Despite no differences in body weight (BW) (Figure 3B), HFD TLR7$^{-/-}$ and TLR9$^{-/-}$ mice showed improved glucose tolerance tests (GTTs) compared with HFD WT littermate controls (Figure 3C). Furthermore, HFD TLR7$^{-/-}$ and TLR9$^{-/-}$ mice had lower fasting insulin (Figure 3D), improvements in insulin tolerance tests (ITTs) (Figure 3E), and decreased VAT fat pad weight (Figure 3F) compared with littermate WT mice. HFD TLR9$^{-/-}$, but not TLR7$^{-/-}$, mice also showed a decrease in liver weights (Figure 3G), as well as decreased hepatic steatosis (Figure S5A). Compared with WT controls, HFD-fed TLR7$^{-/-}$ and TLR9$^{-/-}$ mice had similar maximal $O_2$ consumption (Figure S5B), $CO_2$ output (Figure S5C), respiratory exchange ratio (Figure S5D), energy expenditure (Figure S5E), and food intake (Figure S5F). Acute insulin response studies showed improved adipose insulin signaling in TLR7$^{-/-}$ and TLR9$^{-/-}$ mice and enhanced hepatic insulin signaling in TLR9$^{-/-}$ mice, as indicated by insulin-stimulated phosphorylation of Akt (Figure 3H). In addition, the levels of anti-dsDNA (Figure 3I) and anti-histone (Figure 3J) IgGs were decreased in HFD TLR7$^{-/-}$ and TLR9$^{-/-}$ mice, indicating that these mice are protected from the increased production of autoantibodies against components of ETs observed in HFD WT mice. Compared with their WT controls, NCD-fed TLR7$^{-/-}$ and TLR9$^{-/-}$ mice had similar BW, fasting glucose, GTTs, and ITTs (Figures S5G–S5J). Together these data demonstrate that the endosomal nucleic acid-sensing receptors TLR7 and TLR9 contribute to glucose intolerance and IR during HFD feeding, and they provide an additional means by which aberrant nucleic acid production causes IR in obesity.

### Nucleic Acid-Targeting Pathways Contribute to Immune Cell-Mediated Inflammation in VAT and Liver

Since TLR7 and TLR9 deletion improved metabolic parameters, we hypothesized that resident immune populations expressing these receptors in metabolic tissues would be altered upon HFD feeding in these mice. Both TLR7$^{-/-}$ and TLR9$^{-/-}$ mice had fewer CLSs in VAT (Figures 4A and 4B) and total number of VAT macrophages (Figure 4C). VAT macrophages showed decreased expression of the immune activation marker CD80 (Figure 4D). Furthermore, TLR7$^{-/-}$ mice showed lower percentages of inflammatory M1 and resident M2-polarized macrophages, whereas TLR9$^{-/-}$ mice had a decrease in the percentage of M1 macrophages (Figure 4E).

In addition to macrophages, pDCs selectively express TLR7 and TLR9 and are capable of recognizing autoantibody complexes against nucleic acids. In chronic inflammatory diseases such as SLE, TLR7 and TLR9 facilitate the recognition of autoantibodies against nucleic acids, leading to activation of pDCs and secretion of inflammatory cytokines, including type I interferon (IFN) (Liu and Davidson, 2012). Because the role of pDCs in obesity-induced inflammation has not been investigated, we first determined the total number of pDCs in VAT, liver, and spleen of NCD- and HFD-fed mice. While pDCs were almost undetectable in the VAT, distinct mPDCA-1$^+$ Siglec-H$^+$ pDC populations were
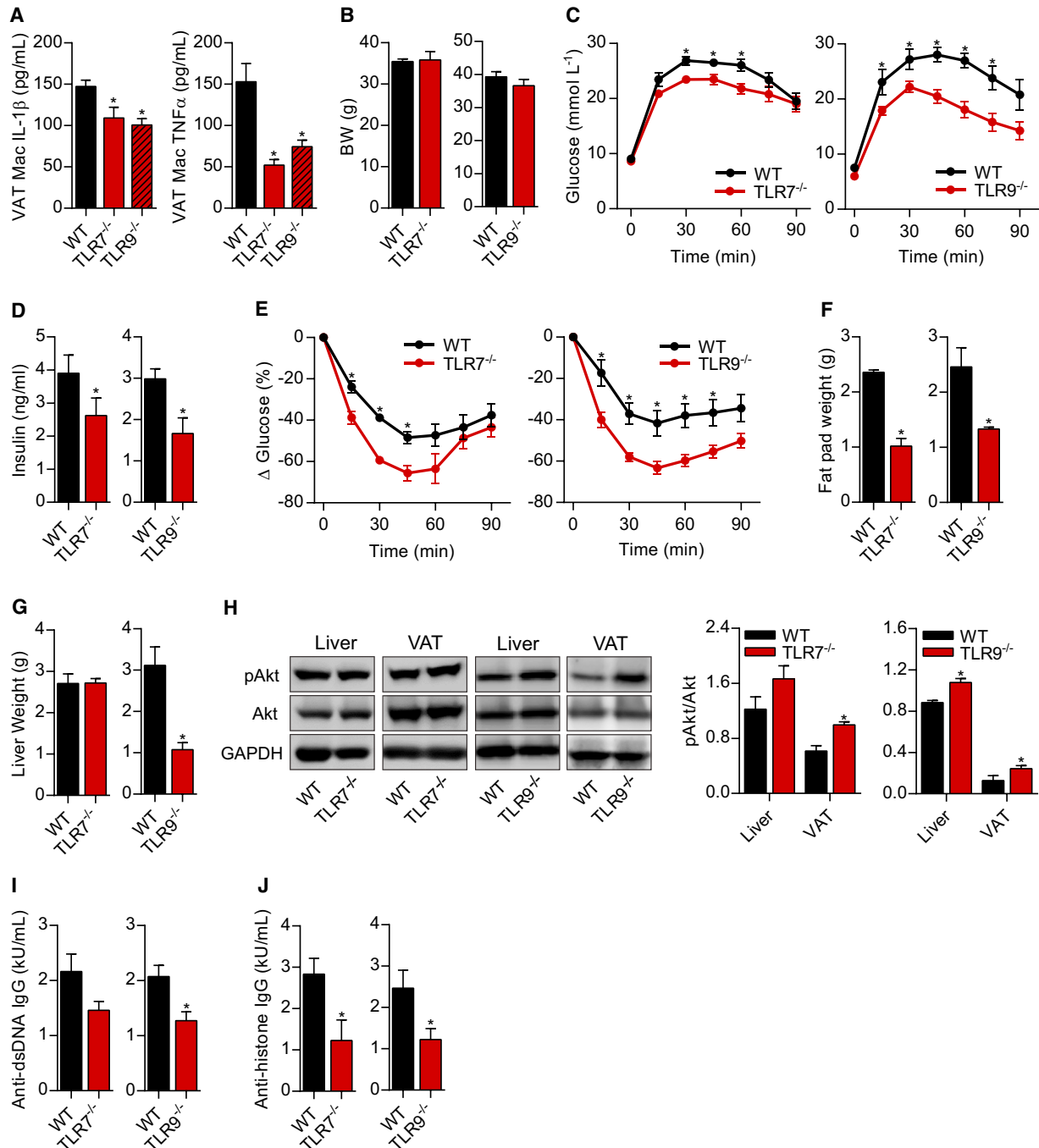
**Figure 3. Genetic Deletion of Nucleic Acid-Sensing Receptors Improves Glucose Homeostasis and Insulin Signaling during HFD Feeding**

(A) Production of IL-1β (left) and TNF-α (right) by VAT macrophages from WT, TLR7$^{-/-}$, and TLR9$^{-/-}$ mice fed an HFD following exposure to purified ETs is shown (n = 10 mice, three experiments, *p < 0.05).

(B–D) Body weights (BWs, B), GTTs (C), and fasting insulin (D) of TLR7$^{-/-}$, TLR9$^{-/-}$, and their WT littermate control mice fed an HFD for 15 weeks are shown (n = 6 for TLR7$^{-/-}$, n = 9 for TLR9$^{-/-}$, n = 6 or 9 for WT mice; *p < 0.05).

(E–G) ITTs (E), gonadal fat pad weights (F), and liver weights (G) of TLR7$^{-/-}$, TLR9$^{-/-}$, and their WT littermate control mice fed an HFD for 15 weeks are shown (n = 5, except in E where n = 6 for TLR7$^{-/-}$, n = 9 for TLR9$^{-/-}$, and n = 6 or 9 for WT mice; *p < 0.05).

(H) Representative western blots (left) and quantification (right) of total and pAkt in liver (n = 7 for TLR7$^{-/-}$, n = 4 for TLR9$^{-/-}$) and VAT (n = 4), after injection of 0.75 or 1.5 units per kg$^{-1}$ i.p. of insulin in HFD-fed WT, TLR7$^{-/-}$, and TLR9$^{-/-}$ mice, are shown (*p < 0.05).

(I and J) Plasma concentrations of anti-dsDNA (I) and anti-histone (J) IgG determined by ELISA in TLR7$^{-/-}$, TLR9$^{-/-}$, and their WT control mice fed an HFD for 15 weeks (n = 5, *p < 0.05). Error bars show mean ± SEM.

See also Figure S5.

identified in the liver and spleen of HFD and NCD mice, with a marked increase in the frequency (Figures S4D and S4E) and numbers (Figure 4F) of pDCs in the liver of HFD-fed mice compared with NCD controls. Notably, HFD mice also showed an increase in the frequency of proinflammatory CCR9⁻ pDCs and a reduction in the frequency of tolerogenic CCR9⁺ pDCs (Hadeiba et al., 2008) in the liver (Figure 4G).

We then assessed pDC populations in TLR7$^{-/-}$ and TLR9$^{-/-}$ mice to examine the possibility that liver pDCs could partly mediate some of the metabolic effects of these TLRs in DIO. Compared with HFD WT controls, both HFD TLR7$^{-/-}$ and TLR9$^{-/-}$ mice had decreased numbers of pDCs in the liver (Figure 4H), with results being more marked in TLR9$^{-/-}$ mice. TLR9-deficient mice also showed a large shift in pDC populations from the pro-inflammatory CCR9⁻ toward the tolerogenic CCR9⁺ phenotype (Figure 4I). As activated pDCs produce large amounts of IFNα, we assessed whether HFD feeding would predispose pDCs to release increased IFNα. Livers from HFD-fed mice had no changes in the frequency (Figure S4F) but a substantial increase in the number of IFNα⁺-producing pDCs (Figure 4J), suggesting that HFD feeding promotes increased activation and accumulation of IFNα-producing pDCs in the liver.

We next determined whether IFNα can directly induce hepatic IR by assessing insulin intracellular signaling in Hepa 1-6 mouse liver cells treated with recombinant IFNα. Hepatocytes treated with IFNα showed a decreased pAkt/Akt protein ratio (Figure 4K), indicating that the cytokine may directly induce IR in liver as a mechanism of action during IR. Because TLR9-deficient, but not TLR7-deficient, mice showed improved insulin signaling in the liver (Figure 3H) and a shift in pDC phenotype (Figure 4I), we determined the number of IFNα⁺ pDCs in the livers of TLR9$^{-/-}$ mice. Consistently, the number of IFNα-producing liver pDCs was decreased in HFD-fed TLR9$^{-/-}$ mice compared with HFD-fed WT controls. Collectively, these findings highlight that changes in the inflammatory and activation statuses of immune populations in metabolic tissues, such as macrophages in the VAT and pDCs in the liver, are directly modulated by nucleic-acid-targeting pathways in obesity-related IR.

### Modulation of Nucleic Acid Ligands Influences Glucose Metabolism

To directly assess the effects of TLR7 and TLR9 agonists on glucose metabolism, 20-week-old NCD mice were injected intraperitoneally (i.p.) with either saline, specific TLR7 ligand imiquimod (IMQ) (Hemmi et al., 2002), or unmethylated CpG DNA TLR9 ligand ODN2395 (ODN) (Bauer et al., 2001). Compared with controls, IMQ- and ODN-injected mice showed no differences in BW (Figure 5A) after 8 days of treatment. ODN, but not IMQ, increased fasting glucose (Figure 5B), although both TLR7 and 9 ligands worsened glucose tolerance (Figure 5C). No changes in fasting insulin were detected (Figure 5D). To investigate whether exogenous IMQ and ODN treatment would influence inflammation in metabolic tissues, we examined their macrophages and pDC populations in the VAT and liver, respectively. IMQ and ODN i.p. injection increased the numbers of CD45⁺ immune cells in VAT (Figure 5E), including a large increase in total macrophages (Figure 5F), consistent with macrophage expression and responsiveness to TLR7 and TLR9 in

mice. In the liver, IMQ and ODN treatments increased the total number of pDCs (Figure 5G) and inflammatory CCR9⁻ pDCs (Figure 5H), although only ODN decreased the number of CCR9⁺ tolerogenic pDCs (Figure 5H). These data suggest that the proinflammatory effects of exogenous IMQ and ODN may be manifested in part by increased numbers of macrophages and proinflammatory pDCs in metabolic tissues.

We next determined if targeting of upstream ET-producing pathways or downstream endosomal receptor pathways could be exploited therapeutically in metabolic disease. Because protein arginine deiminase (PAD)4 is essential for ET formation through histone citrullination (Li et al., 2010; Wang et al., 2009), we treated HFD-fed mice with the PAD4 inhibitor 2-chloroacetamidine (2CA) (Stone et al., 2005) and then assessed their glucose tolerance. HFD-fed mice were treated either with saline or 2CA immediately after the initiation of HFD and up to 10 weeks of HFD feeding. Treatment with 2CA had no effects on BW (Figure 5I), but it impaired ET formation in BM neutrophils and monocytes (Figure S6A). Additionally, 2CA treatment reduced ET formation in VAT macrophages, as determined by H4-Cit3 immunostaining (Figures S6B and S6C). Treatment with 2CA improved glucose tolerance (Figure 5J, left), improved insulin tolerance during an ITT (Figure 5J, right), and reduced fasting insulin (Figure 5K), indicating that interfering with ET formation ameliorates the effects of HFD feeding on whole-body glucose homeostasis. Despite no changes in VAT and liver weights (Figure S6D), 2CA-treated mice showed decreased number of VAT macrophages (Figure S6E) and pDCs in the liver (Figure S6F), suggesting improved tissue inflammatory tone in response to 2CA treatment. Notably, HFD-fed TLR9$^{-/-}$ mice injected with 2CA had no significant improvements in GTT (Figure 5I) and ITT (Figure 5M), suggesting that the effects of 2CA on glucose metabolism are partly mediated by TLR9.

We next aimed to investigate whether targeting TLR7 and TLR9 using the immunoregulatory sequence (IRS) 954 oligonucleotide also would protect HFD-fed mice from metabolic disease. IRS 954 is a dual inhibitor of TLR7 and TLR9 with previous effectiveness in SLE (Barrat et al., 2005) and nonalcoholic steatohepatitis (NASH, Garcia-Martinez et al., 2016). Despite similar weights (Figure 5N, left), obese mice treated with IRS 954 for 3 weeks had improved glucose tolerance (Figure 5N, middle) and a tendency for lower fasting insulin (Figure 5N, right) compared with PBS-injected controls. Furthermore, IRS 954-treated mice showed reduced pDCs in the liver (Figure 5O, left), as well as increased frequency of tolerogenic CCR9⁺ and reduced percentage of proinflammatory CCR9⁻ pDCs (Figure 5O, right), suggesting improved pDC-mediated inflammation in the liver. These data indicate that TLR7 and TLR9 are potential targets for therapeutic agents in the prevention or treatment of obesity-induced IR, and collectively the data highlight nucleic acid-targeting pathways as therapeutic targets in obesity-related IR.

### DISCUSSION

We have identified a fundamental role for nucleic acid-targeting pathways in inflammation associated with DIO. Previous reports have shown that HFD feeding increases neutrophil recruitment
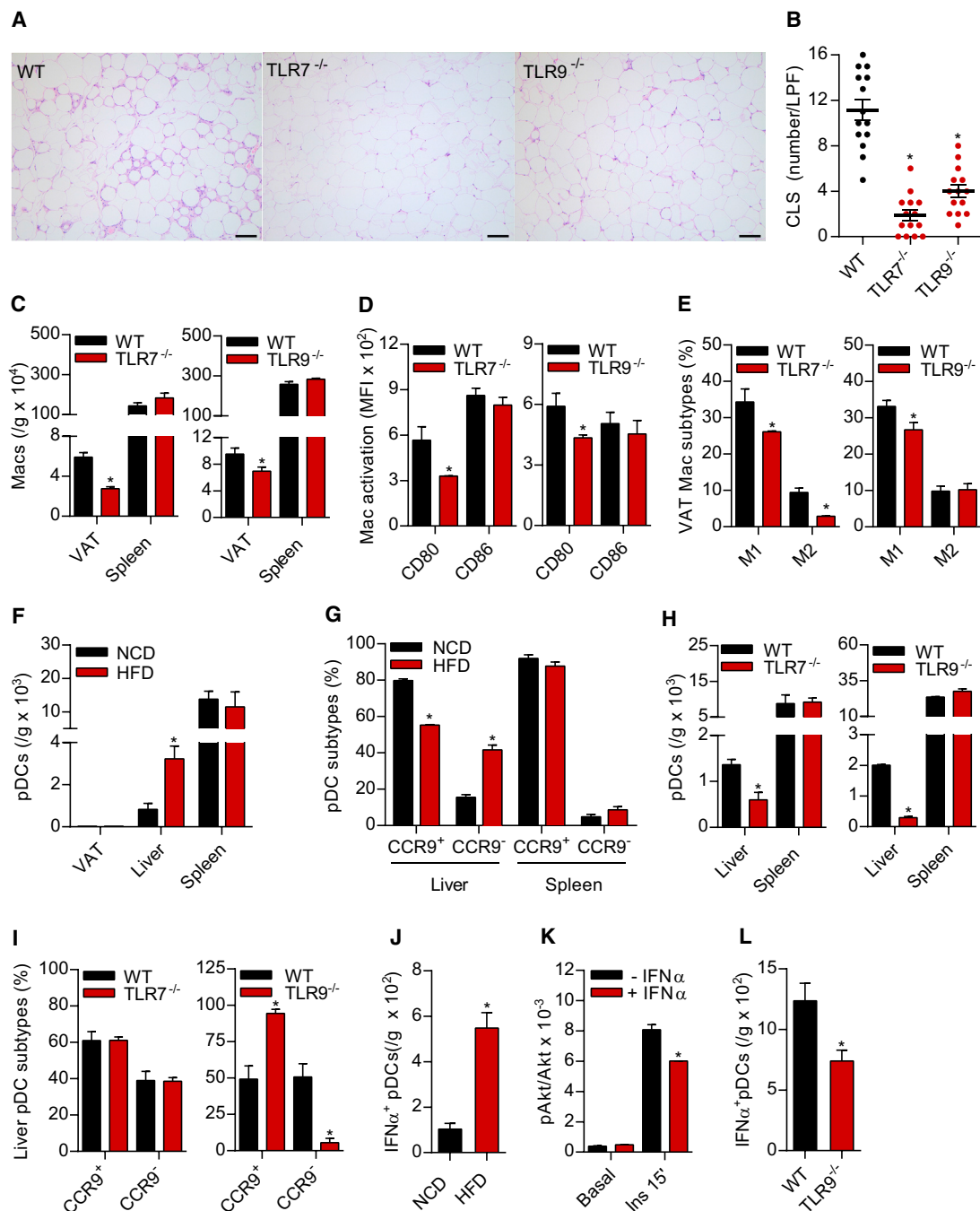
**Figure 4. Macrophages in VAT and Plasmacytoid Dendritic Cells (pDCs) in the Liver Are Cellular Downstream Targets of Nucleic Acid-Targeting Pathways**

(A and B) Representative adipose tissue histology with the scale bar set at 100 μm (A) and counting of crown-like structures (CLSs) per 100× low-power field (LPF, B) from WT, $TLR7^{-/-}$, and $TLR9^{-/-}$ mice fed an HFD for 15 weeks are shown (n = 3 mice, ten LPFs per mouse).

(C–E) Absolute numbers of $F4/80^+$ macrophages (C), expression of the macrophage activation markers CD80 and CD86 (D), and frequency of $CD11c^+CD206^-$ (M1) and $CD11c^-CD206^+$ (M2) macrophages (E) in the VAT (n = 5 mice per group, two experiments, *p < 0.05) of WT, $TLR7^{-/-}$, and $TLR9^{-/-}$ mice fed an HFD for 15 weeks are shown.

(F and G) Absolute numbers of Siglec-$H^+PDCA$-$1^+$ pDCs in the VAT, liver, and spleen (F) and frequency of $CCR9^+$ and $CCR9^-$ pDCs in the liver and spleen (G) of mice fed either an NCD or HFD for 16 weeks are shown (n = 4, *p < 0.05).

(H and I) Absolute numbers of Siglec-$H^+PDCA$-$1^+$ pDCs in the liver and spleen (H) and frequency of $CCR9^+$ and $CCR9^-$ pDCs in the liver (I) of WT, $TLR7^{-/-}$, and $TLR9^{-/-}$ mice fed an HFD for 15 weeks are shown (n = 4, *p < 0.05).

*(legend continued on next page)*

to VAT as early as 3 days upon HFD feeding (Elgazar-Carmon et al., 2008; Talukdar et al., 2012). Here we show that neutrophil numbers also are increased at 15 weeks after the initiation of HFD, implicating a potential role for neutrophils in VAT inflammation during established obesity. As expected, there was also a marked increase in macrophages in VAT during HFD (Mathis, 2013). A central role of phagocytes is their ability to use several antimicrobial mechanisms to eliminate pathogens; however, these same mechanisms also can contribute to tissue injury and amplify pathologic inflammation. In our study, we show that ET formation by phagocytes is augmented systemically and in VAT during HFD feeding.

Increased production and reduced clearance of ETs have been linked to inflammation and are pathogenic mediators of autoimmune diseases, such as SLE (Garcia-Romo et al., 2011; Hakkim et al., 2010), type 1 diabetes (Diana et al., 2013; Wang et al., 2014b), psoriasis (Lin et al., 2011), and vasculitis (Kessenbrock et al., 2009). Recent evidence also indicates that mice and humans with types 1 and 2 diabetes have increased levels of citrullinated histones and formation of ETs, associated with impaired wound healing (Wong et al., 2015). ETs are networks of fibers mainly composed of DNA, histones, and granule proteins (Brinkmann et al., 2004). Citrullination of histones is essential for ET formation (Neeli et al., 2008; Wang et al., 2009). Macrophage ETs recently have been identified within CLSs in mammary gland SAT of mice (Mohanan et al., 2013). We show that VAT macrophages, even in non-stimulated states, have a higher ability to release ET-like structures compared with BM monocytes and that these ETs contribute to VAT inflammation. Given the abundance of macrophages over neutrophils in VAT, METs are likely a dominant promoter of VAT inflammation by ETs.

Increased formation and reduced clearance of ETs can lead to autoantibody overproduction in SLE (Garcia-Romo et al., 2011; Hakkim et al., 2010), and we show that a similar phenomenon occurs in DIO. Disposal of circulating nucleic acids to prevent recognition by innate receptors and consequent inflammation is accomplished partly by nucleases such as DNase (Martínez Valle et al., 2008). The addition of exogenous DNase or MNase restored ET degradation in serum from NCD-fed, but not from HFD-fed, mice, suggesting that ETs are protected from general nuclease activity during obesity. Reduced clearance of ETs likely contributes to the increased levels of autoantibody against conserved nuclear antigens identified in HFD mice, as observed in SLE (Hakkim et al., 2010). In turn, these elevated levels of autoantibodies in HFD-fed mice may block the access of nucleases to ETs. Overall, this mechanism adds to existing work demonstrating augmented production of IgG autoantibody in obesity due to binding of macrophage-derived apoptosis inhibitor of macrophage (AIM) to pentameric IgM complexes (Arai et al., 2013). It was demonstrated previously that HFD-associated B cells are pathogenic in diet-induced IR (Winer et al., 2011). The

identity of the targeted antigens during this aberrant immune response in HFD-fed mice remains unclear. Given the increased levels of autoantibody against conserved nucleoproteins found in this study, some of these antigens might be potential targets, similar to SLE (Barrat et al., 2005). Consistently, increased IgG autoantibody production has been identified in the VAT of lupus-prone mice, providing one possible link between these processes (Gabriel et al., 2012).

Activation of several TLRs, such as TLR2, TLR4, and TLR5, has been directly implicated in the initiation of obesity-induced inflammation. Most notably, TLR4 has been proposed to be a critical link among the consumption of dietary fats, changes in gut microbiota, and metabolic inflammation (Davis et al., 2008; Saberi et al., 2009; Shi et al., 2006). During obesity-induced IR, TLR4 can be activated by dietary factors, such as free fatty acids (Holland et al., 2011), endogenous damage-associated molecular patterns (DAMPs) (Pal et al., 2012), and gut microbiota-derived LPS (Cani et al., 2007; Pussinen et al., 2011). In our study, genetic deletion and IRS 954-mediated inhibition of TLR7 and TLR9 ameliorate the detrimental effects of HFD feeding on glucose metabolism. Previously, TLR9-deficient mice have shown improved IR and reduced steatohepatitis in a model of nonalcoholic fatty liver disease (Miura et al., 2010). In mouse models of SLE, IRS 954 prevented the progression of disease by reducing nucleic acid autoantibodies, serum TNF-α, and macrophage infiltration in kidney (Barrat et al., 2007; Pawar et al., 2007). In agreement with our findings, a very recent study showed that, compared with WT controls, diet-induced obese TLR9-deficient mice have improved insulin tolerance, as TLR9 is involved in the recognition of DNA arising from adipocyte death (Nishimoto et al., 2016). Therefore, targeting TLR7 and TLR9 has promising potential therapeutic application for the treatment of obesity-related IR.

In SLE, TLR7 and TLR9 facilitate the recognition of autoantibodies against nucleic acids and activation of pDCs, which lead to robust secretion of inflammatory cytokines, including type I IFN (Colonna et al., 2004; Liu and Davidson, 2012). Likewise, self-DNA-specific antibody complexes activate TLR9 in pancreatic pDCs, leading to the secretion of IFNα in type 1 diabetes (Diana et al., 2013). In our study, IFNα disrupted insulin signaling in hepatocytes cultured in vitro, suggesting that type I IFN responses can induce IR. However, the potential role of IFNα in mediating IR in DIO requires further investigation using in vivo approaches. Normally, pDCs do not respond robustly to self-DNA, but this tolerance seems to collapse in autoimmune diseases (Gilliet et al., 2008). We show that HFD feeding increases the numbers of pro-inflammatory IFNα-producing pDCs in the liver. These data are consistent with increased loads of TLR7 and TLR9 ligands delivered to the liver in obesity (Henao-Mejia et al., 2012), which could fuel pDC proliferation and activation. Our findings also show that HFD feeding results in a shift from tolerogenic CCR9+ to inflammatory CCR9−

---

(J) Absolute numbers of IFNα+ pDCs in the liver of mice fed either an NCD or HFD for 15 weeks are shown (n = 4, *p < 0.05).

(K) Total Akt and pAkt quantified by mesoscale assay in protein harvested from Hepa 1-6 mouse liver cells after treatment with 100 U/ml recombinant IFNα for 18 hr and spiked with insulin for 15 min to stimulate insulin signaling are shown (triplicates, two experiments, *p < 0.05).

(L) Absolute numbers of IFNα+ pDCs in the liver of WT and TLR9−/− mice fed an HFD for 15 weeks (n = 4, *p < 0.05). Error bars show mean ± SEM.

See also Figure S4.
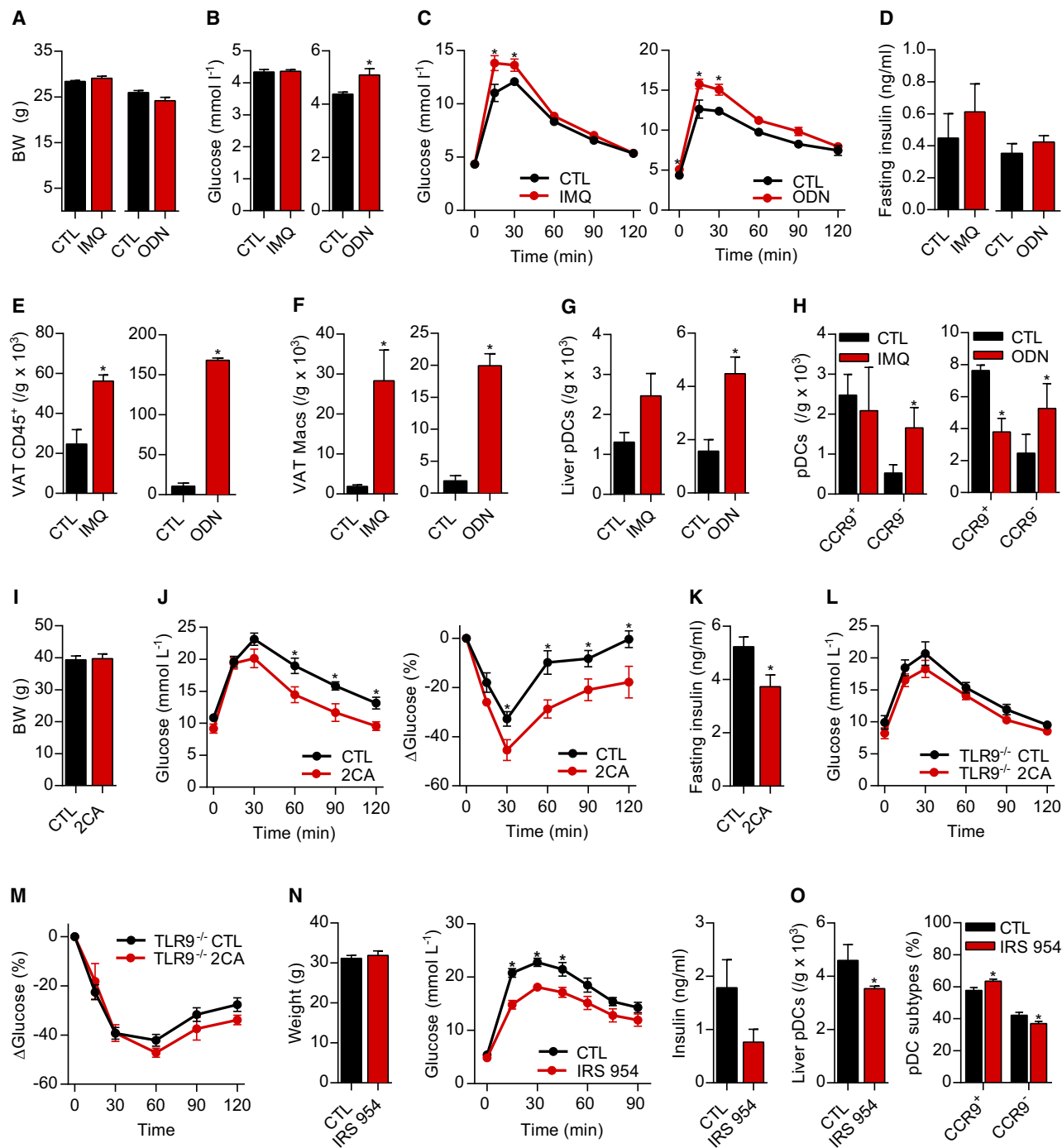
**Figure 5. Targeting Nucleic Acid-Sensing Pathways Alters Glucose Metabolism in Mice**

(A–D) BWs (A), fasting glucose (B), GTT (C), and fasting insulin (D) of 20-week-old NCD mice injected daily for 8 days with 50 µg imiquimod (IMQ, TLR7 ligand), 2 µg CpG ODN2395 (ODN, TLR9 ligand), or saline (CTL) are shown (n = 5, *p < 0.05).

(E and F) Absolute numbers of CD45^{+} immune cells (E) and F4/80^{+} macrophages (F) in the VAT of NCD-fed mice treated with IMQ or ODN are shown (n = 5 mice per group, two experiments, *p < 0.05).

(G and H) Absolute numbers of Siglec-H^{+}PDCA-1^{+} pDCs (G) and numbers (H) of CCR9^{+} and CCR9^{−} pDCs in the liver (n = 3, *p < 0.05) of NCD-fed mice treated with IMQ or ODN are shown.

(I–K) BWs (I), GTT (J, left), ITT (J, right), and fasting insulin (K) of HFD-fed WT mice treated every other day for 10 weeks with either 200 µg PAD inhibitor 2-chloroacetamidine (2CA) or saline (CTL) are shown (n = 5, *p < 0.05).

(L and M) GTT (L) and ITT (M) of HFD-fed TLR9^{−/−} mice treated every other day for 10 weeks with either 200 µg 2CA or saline are shown (n = 5, *p < 0.05).

*(legend continued on next page)*

pDCs that may lead to prolonged inflammation and hepatocyte damage. This inflammatory shift in liver pDCs also potentially could contribute to the worsening state of oral tolerance seen in obesity (Luck et al., 2015). Previous research has shown that CCR9$^+$, but not CCR9$^-$, pDCs potently inhibit antigen-specific immune responses and induce Foxp3$^+$ regulatory T cells (Hadeiba et al., 2008).

Our work suggests that multiple sources of nucleic acids may contribute to glucose intolerance during DIO. First, nucleic acid antigens arising from aberrant formation of ETs can promote inflammation of metabolic tissues through TLR7 and TLR9. A recent study has shown that NETs are enriched in oxidized mitochondrial DNA and promote a type I IFN response in a mouse model of SLE (Lood et al., 2016). Notably, mitochondrial DNA from hepatic origin also is found elevated in the circulation of mice and patients with NASH, and it can promote NASH development via activation of TLR9 (Garcia-Martinez et al., 2016). Thus, it is conceivable that oxidized mitochondrial DNA originating from ETs and/or hepatocytes is one source of TLR9 ligands during diet-induced metabolic disease.

In our study, blocking ET release with the PAD inhibitor 2CA improved glucose homeostasis in WT, but not in TLR9-deficient, HFD-fed mice, implicating excessive nucleic acid release during obesity-induced IR in a process that requires TLR9. Similar to our findings, PAD inhibitors have been shown to reduce citrullination and ameliorate disease in several inflammatory and autoimmune diseases, including SLE (Knight et al., 2015), acute kidney injury (Ham et al., 2014), rheumatoid arthritis (Willis et al., 2011), and multiple sclerosis (Wei et al., 2013) in mice. Hence, hypercitrullination and PAD enzymes may be therapeutic targets in obesity-related inflammation.

Second, it is possible that exogenous sources of nucleic acids, such as CpG motifs found in bacterial DNA, can promote obesity-induced inflammation and IR, as we have shown that a CpG-ODN injection into lean mice worsened glucose tolerance. Emerging evidence has linked alterations in gut microbiota during obesity with IR (Tremaroli and Bäckhed, 2012), and bacterial DNA from intestinal origin has been shown to increase in blood and VAT after 1 week of HFD feeding in mice (Amar et al., 2011). Our findings suggest that, in addition to the LPS/CD14/TLR4 axis (Cani et al., 2007, 2008), obesity-induced changes in gut microbiota may potentially promote IR via recognition of bacterial CpG DNA by TLR9.

Finally, a very recent study has shown that DIO is associated with increased levels of circulating cell-free (cf) DNA, which activates macrophages in a TLR9-dependent manner (Nishimoto et al., 2016). As cultured VAT from HFD-fed mice released more cfDNA compared with NCD-fed controls, the authors suggested that increased cfDNA owes to augmented adipocyte death (Nishimoto et al., 2016), though other sources of nucleic acids likely contribute to circulating cfDNA and TLR9 activation in vivo. Additional studies are needed to pinpoint the relative contributions of these mechanisms in obesity.

Collectively, our data support a pathway of obesity-induced IR in which aberrant production and handling of nucleic acid antigens promote activation of immune cells in metabolic tissues, leading to inflammatory cytokine expression. Increased loads of systemic nuclear antigen are associated with the appearance of autoantibodies against self-antigens in DIO, and they can activate pDCs in the liver via TLR7/9 pathways, inducing their expansion and production of pathogenic type I IFN. Our findings provide evidence of roles for ET, TLR7, and TLR9 signaling in IR, and they highlight the potential benefit of therapies that target pathogenic nucleic acid pathways in DIO.

## EXPERIMENTAL PROCEDURES

### Animals

We purchased C57BL/6J, TLR7$^{-/-}$ (B6.129S1-Tlr7$^{tm1Flv}$/J, backcrossed 11 times to C57BL/6), and TLR9$^{-/-}$ (C57BL/6J-Tlr9$^{M7Btlr}$) mice from The Jackson Laboratory. Heterozygous mice were crossed to generate WT and TLR7 or TLR9 knockout littermates. For the HFD-induced obesity model, mice received either an NCD or HFD (Research Diets, 60 kcal% fat) beginning at 6 weeks of age. Mice were treated with the compounds IMQ/ODN (InvivoGen), 2CA (Sigma), or IRS 954 (Dynavax). All mice were males and age-matched between groups. All experiments were approved by the Institutional Animal Care and Use Committee of University Health Network. For further details, see the Supplemental Experimental Procedures.

### Isolation of Immune Cells from Mouse Tissues

We isolated VAT, spleen, and BM immune cells as previously described (Revelo et al., 2015). See the Supplemental Experimental Procedures.

### Flow Cytometry

Cells were resuspended in PBS containing 2% fetal bovine serum (FBS) and allowed to block nonspecific binding in Fc receptor blocking solution (BioLegend), followed by staining with fluorophore-conjugated primary antibodies. Detection of intracellular IFN$\alpha$ was performed as previously reported (Björck et al., 2011) after liver-derived immune cells were stimulated with or without 10 $\mu$g/ml of ODN2395 (Invivogen) for 9 hr. Data were acquired on a Fortessa flow cytometer (BD Biosciences) and analyzed with FlowJo software (Tree Star). See the Supplemental Experimental Procedures.

### ET Quantification Assay

We measured ET release every 30 min for ∼6 hr using the non-cell-permeant DNA-specific fluorescent dye Sytox Green (Molecular Probes) at a final concentration of 5 $\mu$M. We used a Synergy HT plate reader (BioTek Instruments) to detect fluorescence with excitation/emission wavelengths of 530/580 nm. Plotted fluorescence measurements taken every 30 min were used to calculate areas under the curve (AUCs). See the Supplemental Experimental Procedures.

### ET Immunofluorescence Staining, SEM, and Histology

Isolated monocytes from BM and macrophages from VAT were seeded on glass coverslips in 24-well culture plates and stimulated with 100 ng/ml of LPS for 4 hr (Brinkmann et al., 2010). Specimens were labeled for DNA, elastase, and H4Cit3 and analyzed with a Zeiss LSM700 confocal microscope. SEM was performed by the Microscopy Imaging Lab at the University of Toronto, as previously described (Manzenreiter et al., 2012). Histological sections were stained with H&E and prepared for immunohistochemistry as previously described (Revelo et al., 2015). Immunohistochemical staining of tissue sections from human specimens was approved by the University Health

---

(N and O) BWs (N, left), GTT (N, middle), fasting insulin (N, right), and absolute numbers of Siglec-H$^+$PDCA-1$^+$ liver pDCs (O, left) and frequency of CCR9$^+$ and CCR9$^-$ liver pDCs (O, right) in WT mice fed an HFD for 10 weeks, treated for 3 weeks with either scrambled oligonucleotide control (CTL) or the TLR7/9 antagonist IRS 954 (n = 5, *p < 0.05). Error bars show mean ± SEM.
See also Figure S6.

Network (UHN) Research Ethics Board for Human Subjects. See the Supplemental Experimental Procedures.

### Isolation of ET-Related Proteins and VAT Macrophage Activation

We purified NETs and METs as previously described (Urban et al., 2009). The protein composition of these preparations was determined by MS analysis at the SPARC BioCentre, The Hospital for Sick Children (Data S1). Purified VAT macrophages were primed with 100 ng/ml LPS (Sigma) for 4 hr before exposure to ETs, as previously reported (Kahlenberg et al., 2013). After LPS priming, media were removed, cells were exposed for 2 hr to either purified ETs or RPMI 1640 at 37°C, and supernatants were collected for cytokine assessment. See the Supplemental Experimental Procedures.

### Metabolic Studies

GTTs, ITTs, metabolic cage studies, and measurements of serum insulin were performed as previously described (Revelo et al., 2015).

### Auto-antigen Array

Samples were run on a custom-made auto-antigen array of ∼200 antigens, and they were analyzed by hierarchical clustering (Cluster 3.0) and Statistical Analysis of Microarray (SAM) as previously described (Price et al., 2013).

### Protein ELISA and ELISPOT

ELISA immunoassays were used to measure supernatant concentrations of IL-1β, TNF-α (BioLegend), anti-dsDNA, and -histone IgGs (Alpha Diagnostic International). The frequency of spontaneous IgG-producing B cells in spleen and VAT was determined using a mouse IgG ELISpotPLUS Kit (Mabtech) as previously described (Winer et al., 2011). See the Supplemental Experimental Procedures.

### ANAs in Human Plasma

We obtained plasma samples from 15 normal weight (BMI 24.6 ± 0.6) and nine overweight/obese (BMI 30.6 ± 1.6) subjects enrolled in two studies conducted at the Toronto General Hospital (Dash et al., 2013; Xiao et al., 2014). All patients were male and received no medication at the time of sample collection (Table S1). Human ANAs were detected using a semiquantitative ELISA kit (Alpha Diagnostic International). All human samples were obtained with study approval by the Research Ethics Board for Human Subjects at the UHN. See the Supplemental Experimental Procedures.

### Degradation Assay

BM-derived neutrophils were purified from mice fed an NCD and stimulated to release NETs. Formed NETs were then incubated with 100 U/ml DNase-1 or 10% serum from mice fed either an HFD or NCD. NETs were measured over time using the DNA-specific fluorescent dye Sytox Green, as described in the ET quantification assay. The amount of NET degradation by DNase-1 was considered 100% NET degradation (Hakkim et al., 2010). To determine the presence of DNase-1 and MNase inhibitors, NETs were treated with 10% serum from mice fed either an HFD or NCD spiked with 100 U/ml of either DNase-1 or MNase. See the Supplemental Experimental Procedures.

### Acute Insulin Response and Western Blotting

We fasted mice overnight prior to i.p. injection with 1.5 units/kg insulin. VAT and livers were harvested 15 min after acute insulin injection for quantification of phosphorylated and total Akt (pAkt) by western blotting, as previously described (Revelo et al., 2015). See the Supplemental Experimental Procedures.

### Murine Hepatocytes Culture

Murine liver Hepa 1-6 hepatoma cells were obtained from ATCC (mycoplasma testing pending). We exposed the cells in duplicates for 18 hr to 100 U/ml mouse recombinant IFNα (R&D Systems) in low-glucose medium (Gibco) and 1% FBS. Insulin was added at 10 nM for 15 min and washed once with ice-cold PBS, after which total protein was harvested. Before the addition of insulin, the cells were serum starved for 2 hr. Total Akt and pAkt were measured using a meso scale assay (Meso Scale Discovery) according to the manufacturer's instructions.

### Statistical Analyses

Statistical difference between two means of continuous variables was determined by two-sided unpaired Student's t tests using GraphPad Prism5. In representative datasets, we conducted D'Agostino-Pearson tests to confirm normal distributions using GraphPad Prism5. In figure legends involving multiple experiments from pooled animal tissue, the numbers of mice and biological experiments are listed. Data are presented as means ± SEM. Statistical significance was set at <0.05.

### SUPPLEMENTAL INFORMATION

Supplemental Information includes Supplemental Experimental Procedures, six figures, one table, and one data file and can be found with this article online at http://dx.doi.org/10.1016/j.celrep.2016.06.024.

### REFERENCES

Amar, J., Chabo, C., Waget, A., Klopp, P., Vachoux, C., Bermúdez-Humarán, L.G., Smirnova, N., Bergé, M., Sulpice, T., Lahtinen, S., et al. (2011). Intestinal mucosal adherence and translocation of commensal bacteria at the early onset of type 2 diabetes: molecular mechanisms and probiotic treatment. EMBO Mol. Med. 3, 559–572.

Arai, S., Maehara, N., Iwamura, Y., Honda, S., Nakashima, K., Kai, T., Ogishi, M., Morita, K., Kurokawa, J., Mori, M., et al. (2013). Obesity-associated auto-antibody production requires AIM to retain the immunoglobulin M immune complex on follicular dendritic cells. Cell Rep. 3, 1187–1198.

Barrat, F.J., Meeker, T., Gregorio, J., Chan, J.H., Uematsu, S., Akira, S., Chang, B., Duramad, O., and Coffman, R.L. (2005). Nucleic acids of mammalian origin can act as endogenous ligands for Toll-like receptors and may promote systemic lupus erythematosus. J. Exp. Med. 202, 1131–1139.

Barrat, F.J., Meeker, T., Chan, J.H., Guiducci, C., and Coffman, R.L. (2007). Treatment of lupus-prone mice with a dual inhibitor of TLR7 and TLR9 leads to reduction of autoantibody production and amelioration of disease symptoms. Eur. J. Immunol. 37, 3582–3586.

Bauer, S., Kirschning, C.J., Häcker, H., Redecke, V., Hausmann, S., Akira, S., Wagner, H., and Lipford, G.B. (2001). Human TLR9 confers responsiveness to bacterial DNA via species-specific CpG motif recognition. Proc. Natl. Acad. Sci. USA 98, 9237–9242.

Björck, P., Leong, H.X., and Engleman, E.G. (2011). Plasmacytoid dendritic cell dichotomy: identification of IFN-α producing cells as a phenotypically and functionally distinct subset. J. Immunol. 186, 1477–1485.

Brinkmann, V., Reichard, U., Goosmann, C., Fauler, B., Uhlemann, Y., Weiss, D.S., Weinrauch, Y., and Zychlinsky, A. (2004). Neutrophil extracellular traps kill bacteria. Science 303, 1532–1535.

Brinkmann, V., Laube, B., Abu Abed, U., Goosmann, C., and Zychlinsky, A. (2010). Neutrophil extracellular traps: how to generate and visualize them. J. Vis. Exp. (36), 1724.

Cani, P.D., Amar, J., Iglesias, M.A., Poggi, M., Knauf, C., Bastelica, D., Neyrinck, A.M., Fava, F., Tuohy, K.M., Chabo, C., et al. (2007). Metabolic endotoxemia initiates obesity and insulin resistance. Diabetes 56, 1761–1772.

Cani, P.D., Bibiloni, R., Knauf, C., Waget, A., Neyrinck, A.M., Delzenne, N.M., and Burcelin, R. (2008). Changes in gut microbiota control metabolic endotoxemia-induced inflammation in high-fat diet-induced obesity and diabetes in mice. Diabetes 57, 1470–1481.

Chow, O.A., von Köckritz-Blickwede, M., Bright, A.T., Hensler, M.E., Zinkernagel, A.S., Cogen, A.L., Gallo, R.L., Monestier, M., Wang, Y., Glass, C.K., and Nizet, V. (2010). Statins enhance formation of phagocyte extracellular traps. Cell Host Microbe 8, 445–454.

Colonna, M., Trinchieri, G., and Liu, Y.J. (2004). Plasmacytoid dendritic cells in immunity. Nat. Immunol. 5, 1219–1226.

Dash, S., Xiao, C., Morgantini, C., Szeto, L., and Lewis, G.F. (2013). High-dose resveratrol treatment for 2 weeks inhibits intestinal and hepatic lipoprotein production in overweight/obese men. Arterioscler. Thromb. Vasc. Biol. 33, 2895–2901.

Davis, J.E., Gabler, N.K., Walker-Daniels, J., and Spurlock, M.E. (2008). Tlr-4 deficiency selectively protects against obesity induced by diets high in saturated fat. Obesity (Silver Spring) 16, 1248–1255.

Demir, S., Artim-Esen, B., Şahinkaya, Y., Pehlivan, Ö., Alpay-Kanıtez, N., Omma, A., Erer, B., Kamalı, S., Gül, A., Aral, O., et al. (2016). Metabolic syndrome is not only a risk factor for cardiovascular diseases in systemic lupus erythematosus but is also associated with cumulative organ damage: a cross-sectional analysis of 311 patients. Lupus 25, 177–184.

Diana, J., Simoni, Y., Furio, L., Beaudoin, L., Agerberth, B., Barrat, F., and Lehuen, A. (2013). Crosstalk between neutrophils, B-1a cells and plasmacytoid dendritic cells initiates autoimmune diabetes. Nat. Med. 19, 65–73.

Elgazar-Carmon, V., Rudich, A., Hadad, N., and Levy, R. (2008). Neutrophils transiently infiltrate intra-abdominal fat early in the course of high-fat feeding. J. Lipid Res. 49, 1894–1903.

Gabriel, C.L., Smith, P.B., Mendez-Fernandez, Y.V., Wilhelm, A.J., Ye, A.M., and Major, A.S. (2012). Autoimmune-mediated glucose intolerance in a mouse model of systemic lupus erythematosus. Am. J. Physiol. Endocrinol. Metab. 303, E1313–E1324.

Garcia-Martinez, I., Santoro, N., Chen, Y., Hoque, R., Ouyang, X., Caprio, S., Shlomchik, M.J., Coffman, R.L., Candia, A., and Mehal, W.Z. (2016). Hepatocyte mitochondrial DNA drives nonalcoholic steatohepatitis by activation of TLR9. J. Clin. Invest. 126, 859–864.

Garcia-Romo, G.S., Caielli, S., Vega, B., Connolly, J., Allantaz, F., Xu, Z., Punaro, M., Baisch, J., Guiducci, C., Coffman, R.L., et al. (2011). Netting neutrophils are major inducers of type I IFN production in pediatric systemic lupus erythematosus. Sci. Transl. Med. 3, 73ra20.

Gilliet, M., Cao, W., and Liu, Y.J. (2008). Plasmacytoid dendritic cells: sensing nucleic acids in viral infection and autoimmune diseases. Nat. Rev. Immunol. 8, 594–606.

Hadeiba, H., Sato, T., Habtezion, A., Oderup, C., Pan, J., and Butcher, E.C. (2008). CCR9 expression defines tolerogenic plasmacytoid dendritic cells able to suppress acute graft-versus-host disease. Nat. Immunol. 9, 1253–1260.

Hakkim, A., Fürnrohr, B.G., Amann, K., Laube, B., Abed, U.A., Brinkmann, V., Herrmann, M., Voll, R.E., and Zychlinsky, A. (2010). Impairment of neutrophil extracellular trap degradation is associated with lupus nephritis. Proc. Natl. Acad. Sci. USA 107, 9813–9818.

Ham, A., Rabadi, M., Kim, M., Brown, K.M., Ma, Z., D'Agati, V., and Lee, H.T. (2014). Peptidyl arginine deiminase-4 activation exacerbates kidney ischemia-reperfusion injury. Am. J. Physiol. Renal Physiol. 307, F1052–F1062.

Hemmi, H., Kaisho, T., Takeuchi, O., Sato, S., Sanjo, H., Hoshino, K., Horiuchi, T., Tomizawa, H., Takeda, K., and Akira, S. (2002). Small anti-viral compounds activate immune cells via the TLR7 MyD88-dependent signaling pathway. Nat. Immunol. 3, 196–200.

Henao-Mejia, J., Elinav, E., Jin, C., Hao, L., Mehal, W.Z., Strowig, T., Thaiss, C.A., Kau, A.L., Eisenbarth, S.C., Jurczak, M.J., et al. (2012). Inflammasome-mediated dysbiosis regulates progression of NAFLD and obesity. Nature 482, 179–185.

Holland, W.L., Bikman, B.T., Wang, L.P., Yuguang, G., Sargent, K.M., Bulchand, S., Knotts, T.A., Shui, G., Clegg, D.J., Wenk, M.R., et al. (2011). Lipid-induced insulin resistance mediated by the proinflammatory receptor TLR4 requires saturated fatty acid-induced ceramide biosynthesis in mice. J. Clin. Invest. 121, 1858–1870.

Kahlenberg, J.M., Carmona-Rivera, C., Smith, C.K., and Kaplan, M.J. (2013). Neutrophil extracellular trap-associated protein activation of the NLRP3 inflammasome is enhanced in lupus macrophages. J. Immunol. 190, 1217–1226.

Kessenbrock, K., Krumbholz, M., Schönermarck, U., Back, W., Gross, W.L., Werb, Z., Gröne, H.J., Brinkmann, V., and Jenne, D.E. (2009). Netting neutrophils in autoimmune small-vessel vasculitis. Nat. Med. 15, 623–625.

Knight, J.S., Subramanian, V., O'Dell, A.A., Yalavarthi, S., Zhao, W., Smith, C.K., Hodgin, J.B., Thompson, P.R., and Kaplan, M.J. (2015). Peptidylarginine deiminase inhibition disrupts NET formation and protects against kidney, skin and vascular disease in lupus-prone MRL/lpr mice. Ann. Rheum. Dis. 74, 2199–2206.

Li, P., Li, M., Lindberg, M.R., Kennett, M.J., Xiong, N., and Wang, Y. (2010). PAD4 is essential for antibacterial innate immunity mediated by neutrophil extracellular traps. J. Exp. Med. 207, 1853–1862.

Lin, A.M., Rubin, C.J., Khandpur, R., Wang, J.Y., Riblett, M., Yalavarthi, S., Villanueva, E.C., Shah, P., Kaplan, M.J., and Bruce, A.T. (2011). Mast cells and neutrophils release IL-17 through extracellular trap formation in psoriasis. J. Immunol. 187, 490–500.

Liu, Z., and Davidson, A. (2012). Taming lupus-a new understanding of pathogenesis is leading to clinical advances. Nat. Med. 18, 871–882.

Liu, P., Wu, X., Liao, C., Liu, X., Du, J., Shi, H., Wang, X., Bai, X., Peng, P., Yu, L., et al. (2014). Escherichia coli and Candida albicans induced macrophage extracellular trap-like structures with limited microbicidal activity. PLoS ONE 9, e90042.

Lood, C., Blanco, L.P., Purmalek, M.M., Carmona-Rivera, C., De Ravin, S.S., Smith, C.K., Malech, H.L., Ledbetter, J.A., Elkon, K.B., and Kaplan, M.J. (2016). Neutrophil extracellular traps enriched in oxidized mitochondrial DNA are interferogenic and contribute to lupus-like disease. Nat. Med. 22, 146–153.

Luck, H., Tsai, S., Chung, J., Clemente-Casares, X., Ghazarian, M., Revelo, X.S., Lei, H., Luk, C.T., Shi, S.Y., Surendra, A., et al. (2015). Regulation of obesity-related insulin resistance with gut anti-inflammatory agents. Cell Metab. 21, 527–542.

Manzenreiter, R., Kienberger, F., Marcos, V., Schilcher, K., Krautgartner, W.D., Obermayer, A., Huml, M., Stoiber, W., Hector, A., Griese, M., et al. (2012). Ultrastructural characterization of cystic fibrosis sputum using atomic force and scanning electron microscopy. J. Cyst. Fibros. 11, 84–92.

Martin, D.A., and Elkon, K.B. (2005). Autoantibodies make a U-turn: the toll hypothesis for autoantibody specificity. J. Exp. Med. 202, 1465–1469.

Martínez Valle, F., Balada, E., Ordi-Ros, J., and Vilardell-Tarres, M. (2008). DNase 1 and systemic lupus erythematosus. Autoimmun. Rev. 7, 359–363.

Mathis, D. (2013). Immunological goings-on in visceral adipose tissue. Cell Metab. 17, 851–859.

Miura, K., Kodama, Y., Inokuchi, S., Schnabl, B., Aoyama, T., Ohnishi, H., Olefsky, J.M., Brenner, D.A., and Seki, E. (2010). Toll-like receptor 9 promotes steatohepatitis by induction of interleukin-1beta in mice. Gastroenterology *139*, 323–334.

Mohanan, S., Horibata, S., McElwee, J.L., Dannenberg, A.J., and Coonrod, S.A. (2013). Identification of macrophage extracellular trap-like structures in mammary gland adipose tissue: a preliminary study. Front. Immunol. *4*, 67.

Neeli, I., Khan, S.N., and Radic, M. (2008). Histone deimination as a response to inflammatory stimuli in neutrophils. J. Immunol. *180*, 1895–1902.

Nishimoto, S., Fukuda, D., Higashikuni, Y., Tanaka, K., Hirata, Y., Murata, C., Kim-Kaneyama, J.R., Sato, F., Bando, M., Yagi, S., et al. (2016). Obesity-induced DNA released from adipocytes stimulates chronic adipose tissue inflammation and insulin resistance. Sci. Adv. *2*, e1501332.

Osborn, O., and Olefsky, J.M. (2012). The cellular and signaling networks linking the immune system and metabolism in disease. Nat. Med. *18*, 363–374.

Pal, D., Dasgupta, S., Kundu, R., Maitra, S., Das, G., Mukhopadhyay, S., Ray, S., Majumdar, S.S., and Bhattacharya, S. (2012). Fetuin-A acts as an endogenous ligand of TLR4 to promote lipid-induced insulin resistance. Nat. Med. *18*, 1279–1285.

Parker, B., and Bruce, I.N. (2010). The metabolic syndrome in systemic lupus erythematosus. Rheum. Dis. Clin. North Am. *36*, 81–97, viii.

Parker, B., Urowitz, M.B., Gladman, D.D., Lunt, M., Donn, R., Bae, S.C., Sanchez-Guerrero, J., Romero-Diaz, J., Gordon, C., Wallace, D.J., et al. (2015). Impact of early disease factors on metabolic syndrome in systemic lupus erythematosus: data from an international inception cohort. Ann. Rheum. Dis. *74*, 1530–1536.

Pawar, R.D., Ramanjaneyulu, A., Kulkarni, O.P., Lech, M., Segerer, S., and Anders, H.J. (2007). Inhibition of Toll-like receptor-7 (TLR-7) or TLR-7 plus TLR-9 attenuates glomerulonephritis and lung injury in experimental lupus. J. Am. Soc. Nephrol. *18*, 1721–1731.

Price, J.V., Haddon, D.J., Kemmer, D., Delepine, G., Mandelbaum, G., Jarrell, J.A., Gupta, R., Balboni, I., Chakravarty, E.F., Sokolove, J., et al. (2013). Protein microarray analysis reveals BAFF-binding autoantibodies in systemic lupus erythematosus. J. Clin. Invest. *123*, 5135–5145.

Pussinen, P.J., Havulinna, A.S., Lehto, M., Sundvall, J., and Salomaa, V. (2011). Endotoxemia is associated with an increased risk of incident diabetes. Diabetes Care *34*, 392–397.

Revelo, X.S., Tsai, S., Lei, H., Luck, H., Ghazarian, M., Tsui, H., Shi, S.Y., Schroer, S., Luk, C.T., Lin, G.H., et al. (2015). Perforin is a novel immune regulator of obesity-related insulin resistance. Diabetes *64*, 90–103.

Saberi, M., Woods, N.B., de Luca, C., Schenk, S., Lu, J.C., Bandyopadhyay, G., Verma, I.M., and Olefsky, J.M. (2009). Hematopoietic cell-specific deletion of toll-like receptor 4 ameliorates hepatic and adipose tissue insulin resistance in high-fat-fed mice. Cell Metab. *10*, 419–429.

Savarese, E., Chae, O.W., Trowitzsch, S., Weber, G., Kastner, B., Akira, S., Wagner, H., Schmid, R.M., Bauer, S., and Krug, A. (2006). U1 small nuclear ribonucleoprotein immune complexes induce type I interferon in plasmacytoid dendritic cells through TLR7. Blood *107*, 3229–3234.

Shi, H., Kokoeva, M.V., Inouye, K., Tzameli, I., Yin, H., and Flier, J.S. (2006). TLR4 links innate immunity and fatty acid-induced insulin resistance. J. Clin. Invest. *116*, 3015–3025.

Stone, E.M., Schaller, T.H., Bianchi, H., Person, M.D., and Fast, W. (2005). Inactivation of two diverse enzymes in the amidinotransferase superfamily by 2-chloroacetamidine: dimethylargininase and peptidylarginine deiminase. Biochemistry *44*, 13744–13752.

Talukdar, S., Oh, Y., Bandyopadhyay, G., Li, D., Xu, J., McNelis, J., Lu, M., Li, P., Yan, Q., Zhu, Y., et al. (2012). Neutrophils mediate insulin resistance in mice fed a high-fat diet through secreted elastase. Nat. Med. *18*, 1407–1412.

Tillack, K., Breiden, P., Martin, R., and Sospedra, M. (2012). T lymphocyte priming by neutrophil extracellular traps links innate and adaptive immune responses. J. Immunol. *188*, 3150–3159.

Tremaroli, V., and Bäckhed, F. (2012). Functional interactions between the gut microbiota and host metabolism. Nature *489*, 242–249.

Urban, C.F., Ermert, D., Schmid, M., Abu-Abed, U., Goosmann, C., Nacken, W., Brinkmann, V., Jungblut, P.R., and Zychlinsky, A. (2009). Neutrophil extracellular traps contain calprotectin, a cytosolic protein complex involved in host defense against Candida albicans. PLoS Pathog. *5*, e1000639.

Wang, Y., Li, M., Stadler, S., Correll, S., Li, P., Wang, D., Hayama, R., Leonelli, L., Han, H., Grigoryev, S.A., et al. (2009). Histone hypercitrullination mediates chromatin decondensation and neutrophil extracellular trap formation. J. Cell Biol. *184*, 205–213.

Wang, Q., Xie, Z., Zhang, W., Zhou, J., Wu, Y., Zhang, M., Zhu, H., and Zou, M.H. (2014a). Myeloperoxidase deletion prevents high-fat diet-induced obesity and insulin resistance. Diabetes *63*, 4172–4185.

Wang, Y., Xiao, Y., Zhong, L., Ye, D., Zhang, J., Tu, Y., Bornstein, S.R., Zhou, Z., Lam, K.S., and Xu, A. (2014b). Increased neutrophil elastase and proteinase 3 and augmented NETosis are closely associated with β-cell autoimmunity in patients with type 1 diabetes. Diabetes *63*, 4239–4248.

Webster, S.J., Daigneault, M., Bewley, M.A., Preston, J.A., Marriott, H.M., Walmsley, S.R., Read, R.C., Whyte, M.K., and Dockrell, D.H. (2010). Distinct cell death programs in monocytes regulate innate responses following challenge with common causes of invasive bacterial disease. J. Immunol. *185*, 2968–2979.

Wei, L., Wasilewski, E., Chakka, S.K., Bello, A.M., Moscarello, M.A., and Kotra, L.P. (2013). Novel inhibitors of protein arginine deiminase with potential activity in multiple sclerosis animal model. J. Med. Chem. *56*, 1715–1722.

Willis, V.C., Gizinski, A.M., Banda, N.K., Causey, C.P., Knuckley, B., Cordova, K.N., Luo, Y., Levitt, B., Glogowska, M., Chandra, P., et al. (2011). N-α-benzoyl-N5-(2-chloro-1-iminoethyl)-L-ornithine amide, a protein arginine deiminase inhibitor, reduces the severity of murine collagen-induced arthritis. J. Immunol. *186*, 4396–4404.

Winer, D.A., Winer, S., Shen, L., Wadia, P.P., Yantha, J., Paltser, G., Tsui, H., Wu, P., Davidson, M.G., Alonso, M.N., et al. (2011). B cells promote insulin resistance through modulation of T cells and production of pathogenic IgG antibodies. Nat. Med. *17*, 610–617.

Wong, S.L., Demers, M., Martinod, K., Gallant, M., Wang, Y., Goldfine, A.B., Kahn, C.R., and Wagner, D.D. (2015). Diabetes primes neutrophils to undergo NETosis, which impairs wound healing. Nat. Med. *21*, 815–819.

Xiao, C., Dash, S., Morgantini, C., Patterson, B.W., and Lewis, G.F. (2014). Sitagliptin, a DPP-4 inhibitor, acutely inhibits intestinal lipoprotein particle secretion in healthy humans. Diabetes *63*, 2394–2401.